All-Aqueous Freeform Fabrication of Perfusable Self-Standing Soft Compartments

Raquel C. Gonçalves, Sara Vilabril, Catarina M. S. S. Neves, Mara G. Freire, João A. P. Coutinho, Mariana B. Oliveira, João F. Mano**

R.C. Gonçalves, S. Vilabril, C.M.S.S. Neves, M.G. Freire, J.A.P. Coutinho, M.B. Oliveira, J.F. Mano
Department of Chemistry, CICECO – Aveiro Institute of Materials. University of Aveiro. 3810-193 Aveiro, Portugal
E-mail: mboliveira@ua.pt, jmano@ua.pt

Keywords: all-aqueous fabrication, tubular/hollow materials, aqueous two-phase systems, interfacial complexation, cell encapsulation

Abstract. Compartmentalized structures obtained in all-aqueous settings have shown promising properties as cell encapsulation devices, as well as reactors for trans-membrane chemical reactions. While most approaches focus on the preparation of spherical devices, advances on the production of complex architectures have been enabled by the interfacial stability conferred by emulsion systems, namely mild aqueous two-phase systems (ATPS), or non-equilibrated analogues. However, the application of non-spherical structures has mostly been reported while keeping the fabricated materials at a stable interface, limiting the free-standing character, mobility, and transposition of the obtained structures to different setups. Here, we show the fabrication of self-standing, malleable and perfusable tubular systems through all-aqueous interfacial assembly, culminating in the preparation of independent objects with stability and homogeneity after disruption of the polymer-based aqueous separating system. Those hollow structures could be fabricated with a variety of widths, and rapidly printed as long structures at flow rates of 15 mm s^{-1}. The materials were used as compartments for cell culture, showcasing high cytocompatibility, and could be tailored to promote cell adhesion. Such structures may find application in fields that benefit from freeform tubular structures, including the biomedical field with e.g., cell encapsulation, and benchtop preparation of microfluidic devices.

1. Introduction

Strategies with high relevance in the biotechnology and bioengineering fields, including drug/protein delivery and enzyme immobilization, have relied on compartmentalization approaches compatible with mild processing.[1] Such encapsulation methods have been adapted and extended to withstand cell encapsulation, relevant for tissue engineering and regenerative medicine, and to recent technological developments on disease modelling.[2] Most emphasis has been given to spherical-shaped cell encapsulation systems due to ease of processing, as well as to the architecture-enabled achievement of controlled molecular release profiles. More recently, though, fibrillar and tubular geometries have gained momentum, mainly owing to their ability to mimic complex and hierarchical architectures of naturally occurring fiber-shaped and tubular tissues including, for example, vasculature.[2,3] Also, flexible fiber-shaped materials may be deposited with high three-dimensional (3D) freedom, enabling the bottom-up fabrication of complex geometries, much needed in tissue regeneration based on defect-filling strategies.[4,5] Other biomedical-related applications may reside in their integration on fluidics models[6] or as platforms for the generation of organoid models.[7,8]

The direct fabrication of perfusable tubular materials with free-form distributions may arise from techniques such as co-axial extrusion 3D printing. Those often require the use of one phase that gives rise to sacrificial templates that need subsequential removal with, for example, ion chelating agents.[9–13] On the other hand, all-liquid template-free strategies are most commonly based on the assembly of a variety of active materials such as surfactants[14] or nanoparticles[15] at oil-aqueous interfaces.[16] However, traces of oil or organic solvents may be either difficult to wash and/or pose toxicity constrains. Aqueous two-phase systems (ATPS) have emerged as interesting platforms to fabricate emulsion-based structures in all-aqueous environments. The aqueous environment provided by these systems has led to their application in the processing of products for the tissue engineering and biomedical field.[17] ATPS are formed when two aqueous solutions containing incompatible polymers, salts or other agents, separate into two immiscible phases above certain critical concentrations.[18] Dispersing oppositely charged polyelectrolytes (PEs) in the different phases of the ATPS or their analogues has been explored as a way to produce biomaterials through a single-step interfacial complexation. This method has been mainly used for the generation of PE spherical-shaped capsules and particles with potential applications in cell encapsulation, controlled release of active agents[19–23] and, more recently, for the fabrication of disease models.[24] The processing of such structures in tubular form through PE complexation is poorly explored[25]. The few studies reporting the fabrication of complex-shaped materials at the interface of all-aqueous

interfaces have proven their applicability as supports for intermembranous reactions[25] and cell encapsulation[4] while kept at the stabilized ATPS, or "prototypical" ATPS interfaces based on non-equilibrium analogues[25]. The effect of either using ATPS in equilibrium – as well as in different equilibrium points -, or prototypical systems based on precursory aqueous polymer solutions before equilibration, has been overlooked. Importantly, the ability of all-aqueous systems to assist on the fabrication of materials with architectural complexity, homogeneity, and ability to be handled after disruption of the interface remains unexplored. This has limited the technique for the production of materials amenable to be independently handled and positioned in more complex systems.

Here, we report the direct and rapid fabrication of perfusable fiber-shaped materials supported by the well-characterized ATPS composed of poly(ethylene glycol) (PEG) and dextran. By adjusting physical and chemical processing parameters, namely by exploring non-equilibrium and different equilibrium points of the ATPS, we prove the feasibility of processing self-standing, easy to handle and cytocompatible materials with membrane-bounded tubular shape.

2. Results and discussion

The interfacial complexation of two oppositely charged natural PEs – alginate (ALG) and ε-poly-L-lysine (EPL) –, at physiological pH (7.2-7.4), was promoted at the interface of different aqueous systems. In an initial experiment, a system based on an ATPS precursor composed of aqueous PEG and dextran solutions was thoroughly characterized. For that, ALG was dissolved in a 15 wt% dextran solution (phase I – inner phase) and immersed in a larger volume solution made of EPL dissolved in a 17 wt% PEG solution (phase II – outer phase) (**Figure 1**a). The formation of tubular structures was induced by dispensing a discrete phase (phase I) into a continuous bath (phase II) by applying controlled continuous displacement.

The interaction between oppositely charged PEs was crucial for the development of stable structures: when a PE-free phase I was immersed in a PE-free phase II, long threads were formed upon the application of movement. However, the thread broke up into smaller droplets within less than 1 minute (Table S1, Supporting Information).[17] When oppositely-charged PEs were dissolved in the solutions, a condensed membrane was formed, which can probably be ascribed to the electrostatic interaction between the charged groups of the polymers, as well as the entropy gain upon the release of counter ions and solvating molecules in solution, in a phenomenon called PE complexation.[26,27] Previous studies using PE complexation in ATPS to produce biomaterials demonstrated that the phase in which the PEs are initially positioned

may influence the formed structure, as well as the ability to fabricate continuous materials with high stability while kept at the ATPS precursor interface.[25,28] In an initial approach, we empirically investigated the effect of inversing the dissolution of both PEs in the phases. Macroscopic observations showed the formation of continuous and surface-homogeneous fibers when alginate was mixed in the inner phase (dextran), and EPL in the outer one (PEG). On the other hand, disintegrated structures were obtained when alginate and EPL were in the outer and inner phases, respectively (Figure S1, Supporting Information).

By using the optimized phase positioning and initially studied concentrations of 0.75 wt% EPL and 2 wt% ALG, the formation of a detectable membrane at the interface around the immersed phase took around 30 seconds (Figure 1b). Due to the aqueous nature of the system, the dissolved PEs are hypothesized to slowly diffuse towards the interface of the ATPS precursor. Overtime, polyions are expected to continuously interact, which correlates with the gradually increasingly darkening of the membrane, and the consequent formation of more robust fiber-shaped structures (Figure 1b,c). Interestingly, in the absence of the precursor ATPS, the reaction between EPL and ALG (dissolved in PBS) led to the formation of structures with poor malleability (Videos S1 and S2, Supporting Information), which were darker at 2 min of complexation than any of the structures prepared using the ATPS precursor, regardless of complexation time. Additionally, the gradual increase in the darkness observed for the materials prepared in the non-equilibrium ATPS was not detectable in the non-equilibrium ATPS-free setup, suggesting that the use of a non-equilibrated ATPS enable establishing time of complexation as a parameter to easily induce morphological versatility in the prepared membranes/tubes (Figure 1c). Since the membrane was formed at the interface of the aqueous system, ones would expect that, by cutting off the ends of the materials, the produced fibers would be hollow upon releasing their liquid content, producing tubular structures. Scanning electron microscopy (SEM) micrographs of cross-sectioned and dehydrated fibers with different complexation times allowed confirming the tubular/hollow feature of the fabricated structures (Figure 1d).

Upon the disruption of the interface of the ATPS precursor, fiber-shaped solid structures were retrieved to a saline medium without visible collapse (Figure 1e). Interestingly, the free-standing structures showed robustness and could be easily handled with tweezers both in a water-based solution, as well as while in contact with air (Figure 1f,g). The microscopic analysis of the membranes right after production and cross-sectioning allowed estimating a thickness c.a. 7-12 μm, with a slight increase on walls' thickness with increasing complexation time (Figure S2a, Supporting Information).

A volumetric expansion of the fibers was observed upon washing in PBS, which was hypothesized to be triggered by the disruption of the interfacial tension barrier from the ATPS after complete removal of phase II during the washing. The disturbance of the aqueous interface may had established osmotic gradients that induced the movement of water molecules towards the interior of the fibers, culminating in swelling.[23] The expansion process was monitored over time by registering the changes in fibers' diameter (Figure S2b, Supporting Information). The average swelling ratio increased with time, and eventually reached equilibrium after 40 min for all conditions. Moreover, fibers washed after a reduced time of complexation (2 and 5 min) expanded in a higher extent than fibers with 10 and 15 min of complexation. As mechanical analysis corroborates, lower complexation times led to the formation of softer fibers; therefore, their membrane may more easily deform, and fibers expand more upon the entrance of water, while stiffer fibers resist more to expansion resulting in lower swelling ratios. A tendency for increasing elastic modulus with the increase in the complexation time was observed. Statistically significant difference of almost two-fold was detected between 5 min (15 ± 0.7 kPa) and 15 min (27 ± 1.9 kPa), with fibers with increasing stiffness produced with increased complexation times (Figure S2c, Supporting Information). The PE complexation has been described to be mostly entropically driven, with a two-phase sequence firstly involving formation of soluble complexes, and a second step involving coacervation (comprising water expulsion), driving the formation of insoluble organized complexes.[29] We speculated the stiffening of the membranes formed at the interface of the system may be related with the decreased hydration of the membranes as complexation time increases, as well as a putative progressive organization of the coacervates. Therefore, softer fibers may have been obtained from lower times of complexation due to their ability to retain and absorb higher amounts of water. Using this system, the mechanical performance of fibers could be easily tuned by the complexation time, presenting a range of stiffnesses resembling some native soft tissues such as cardiac and skeletal muscle[30], providing them with potential for cell support and tissue integration. The diameter of the fibers could easily be tuned by changing the needle used to deposit phase I into phase II. Due to their water-swelling properties, the diameter significantly increased for all the tested needle sizes after the washing process (Figure S2d, Supporting Information). This approach allowed stablishing a range of low-dispersion external diameters comprising macrometer (1.50 ± 0.19 mm) to micrometer scales (0.25 ± 0.03 mm), opening the range of applications for the system.

Despite the tubular shape and handelability obtained for the studied times of complexation using 0.75 wt% EPL and 2 wt% ALG in the ATPS precursor, the microscopic

observation of the obtained tubes after washing revealed uncontinuities in the membranes (**Figure 2**a,b), especially for the ones produced using higher complexation times. Therefore, a more thorough study of processing conditions comprising different polymer concentrations, times of complexation, and the pH of the solutions was performed. The yield of fibers that kept a continuous character, without microscopically detectable opening or collapsing after washing with PBS, followed by incubation at 37ºC overnight, was calculated. Fibers were prepared using a syringe pump system, which allowed controlling the flow rate of phase I, and achieve increased reproducibility when compared to manual dispensing of solutions. Figure 2c summarizes the stability yield obtained for all tested conditions, with solutions prepared at pH ~7. A tendency for decreasing stability with increasing complexation times seems to occur, regardless of PE concentrations. Beyond the attractive electrostatic interactions, the entropy gain from the release of water is considered to be one of the driving forces for the formation of PE complexes or coacervates.[26] In fact, it has been previously described that the presence of highly hydrophilic polymers in solutions with oppositely charged PEs, enhance the dehydration of the PE constituents and favors entropically the formation of the coacervation condensate.[31] We therefore hypothesized that, with increasing time, the increasing PE interactions and consequent dehydration of the PE molecules and possible local accumulation of elastic stress[32] may have caused the tightening of the membrane mesh, inducing the opening of thermodynamically instable areas of the fiber. The fact that an ATPS precursor, in a non-equilibrium state, was used to prepare the fibers may explain the formation of localized sites with accumulated elastic stress in the forming fibers. The time for the first breakage of the PE-free precursor ATPS was assessed, with the first breakage being detected in less than 1 minute after the filament extrusion (Table S1, Supporting Information).

Both alginate and EPL are weak polyelectrolytes, with a degree of ionization in solution dependent on a dissociation constant, pKa.[33] This property enables polymers to acquire fractional charges, which can be tuned by changing the solution's pH.[34] Taking this aspect in consideration, we evaluated the role of pH on the formation and stability of fiber-shaped materials. More robust fibers were formed when the pH of the global system decreased to 5, while increasing the pH to 9 prevented the formation of fibers (Figure 2d). This result was deemed to be mainly influenced by the degree of protonation and conformation of EPL, since the charge density of alginate (pKa ~ 3.2-3.6)[35] was previously shown not to be significantly influenced by solutions' pH above 5.[36] At acidic pH, the repulsion of protonated amine groups of EPL might promote an electrostatically expanded conformation[37] which favors the interaction with the carboxylic groups from alginate, thereby increasing the speed of

complexation (Figure 2d). Theoretically, EPL isoelectric point is assumed to be close to 9[38]; consequently, interfacial electrostatic interactions between the PEs at pH 9 is expected to be mostly absent, which here may had prevented the formation of complexed membranes. This was corroborated by the higher transparency of the formed fibers at pH 9 (Figure 2d). Considering these findings, the yield of structures capable of preserving their tubular features after washing and overnight incubation was calculated for fibers obtained using phases at different pH values (Figure 2e). As expected, a generalized decrease in stability with increasing pH of phase II, where EPL was dissolved, was observed. When the EPL-containing phase was kept at pH 5, the interfacial membrane formed more quickly yielding highly stable structures. However, even with the EPL-containing phase at pH 5, an increase in phase I (alginate-containing phase) to 9 led to the formation of less stable membranes. In fact, the assembly of PEs in an ATPS depends not only on the electrostatic interaction between the PE's charged groups, but it is also critically influenced by the affinity and partitioning-induced distribution of the PEs in the distinct polymer phases.[39] Based on the theory purposed by Ma *et al.* which states that an increase in pH may enhance hydrogen bonds between polyelectrolytes and the hydroxyl groups of dextran[39], we hypothesize that higher pH values in our solutions could have increased the affinity of alginate towards the dissolving phase. Consequently, its availability at the interface would be decreased, culminating in the reduced stability of the produced fibers. In summary, it was possible to control the formation and stability of the fiber-shaped structures, mostly by charge- and time-dependent mechanisms (Figure 2f), and possibly by ATPS-PEs, by tuning the pH of the system.

Moreover, the stability of washed fibers, produced in 2 minutes of complexation, when immersed in solutions at different pH, was evaluated (Figure S3, Supporting Information). Low pH values, including 1 and 4, induced the stiffening of the fibers, while alkaline pH values in the range of 10 and 13 led to the loss of integrity of the fibers. A very speedy effect observed for pH 13, with the complete disintegration of the fibers within a few seconds. The structural loss of the fibers at pH 13 may be ascribed to the loss of charge from amines in EPL, as well as possible acquisition of negative charge (owing to carboxyl groups), culminating in increased repulsion between EPL and ALG.

An overall analysis of processing conditions allowed stablishing ALG and EPL concentrations of 2 wt% and 0.75 wt%, with 2 min of complexation and pH~7, as the most robust condition for further functional characterization. The processing conditions comprising close-to-physiological pH, the use of an isotonic solution to dissolve the polymers, as well as the short time of complexation, also made these structures appealing as devices for the mild

encapsulation processes. Therefore, the selected condition was explored on its permeability and adequacy to withstand cell culture.

The possibility to develop compartmentalized tubular systems with adequate permeability is crucial to ensure long-term survival of encapsulated biological compounds, and to possibly improve the system's ability to serve as a permselective releasing and uptaking container. The permeability of fibers was assessed using FITC-dextran molecules with different molecular weights (40 and 150 kDa), as well as FITC-albumin (~67 kDa) as a representative protein model. The fluorescent molecules were dissolved in the inner phase (DEX+ALG), and fibers were produced and washed. Fluorescence intensity inside the material was monitored for a 24h period. All molecules could diffuse through the membrane over time, with a high decrease of fluorescence intensity after 60 min (Figure 2g). This release profile suggests that most molecular content was probably released through a burst release, indicating their free diffusion through the membrane. Negligible fluorescence was observed after 60 min for albumin and small sized dextran molecules (Figure S4a, Supporting Information), indicating the permeability of the membrane material to small molecules and proteins, suggesting its effectiveness in exchanging nutrients, oxygen and metabolites essential for cell function and survival. In opposition, fibers prepared in the absence of the ATPS precursor (PEs dissolved in PBS) showed low permeability to molecules as small as 10 kDa for four hours (Figure S4b, Supporting Information), indicating that a further release may have been set by an increase on membranes' permeability by, for example, swelling mechanisms or occurrence of localized defects due to osmotic pressure.

To demonstrate the versatility of the developed system, the ability of the developed tubes to be perfused with aqueous solutions was examined by injecting a blue dye solution using a syringe. Perfusing liquids directly through bioengineered constructs is considered a key requirement for the generation of functional tubular tissues.[12] The entire length of the materials could be perfused with flows ranging from 2 µl min^{-1} to 2 ml min^{-1} - in ranges frequently used in microfluidics for biomaterials processing, cell mechanical stimulation, and cell sorting applications[40,41]; Video S3) -, and continuously up to 1 hour (Video S4), while keeping their structural integrity (Figure 2h). Moreover, the absence of a pre-formed solid template enabled the easy development of free-form configurations using an extrusion 3D bioprinter (Figure 2i; Video S5, Supporting Information). The deposition of phase I into phase II was achieved in multiple directions, giving this method the potential to be used in the fabrication of fit-to-shape materials to fill pre-determined shapes, such as tissue defects.[5] Bioprinting of such tubule

fibers offers easy control not only over the geometry and distribution, but also the length, enabling the generation of structures with virtually unlimited length (Figure 2i).

Regardless of the concentrations of PE used for the formation of fibers, the fabrication of non-leaky structures at the interface of the non-equilibrated ATPS was dependent on the control over PE complexation time, with best yields obtained for 2 minutes. We hypothesized that the formation of leaky regions at the coacervated membranes could be ascribed to increasing tensions formed at tendentially breaking points of the filament, which occurred at times lower than 1 minute for PE-free solutions. The use of equilibrated ATPS (**Figure 3**a) was hypothesized to render more stable interfaces. Additionally, the variation of different equilibrium points – corresponding to different tie lines in the phase separation diagram of the ATPS (Figure 3b) – enables selecting working points with varying interfacial tensions.[42] Considering such versatility, the effect of using ATPS points corresponding to tie lines (TL) with increasing distance to the binodal curve was assessed. Since the PEG/dextran system has been well characterized in the literature, data reported by Liu et al.[42] were used to approximately characterize the binodal curve, and further select tie lines. Filaments of dextran or dextran-rich (equilibrated) phases were dispensed in PEG or PEG-rich (equilibrated) baths using a 3D bioprinter (Table S1, Supporting Information). The time after initiating extrusion (i.e., with the system at rest after full filament deposition) until the first breakage was registered. Conditions prepared in equilibrated phases showed the first breakage at later times when compared to the non-equilibrated phases. The tendency for breakage was attenuated and delayed for TLs associated with lower interfacial tension (i.e., time for breakage of TL1 > TL2 > TL3), with values for TL1 c.a. 5 minutes until the first breakage.

To further characterize the overall system, we calculated the partition coefficients for the three different ATPS compositions (Figure 3c). Overall, ALG showed a stronger affinity for the dextran-rich phases, while EPL also partitioned preferentially towards the same phase, with affinity for dextran in the following order: TL3 > TL2 > TL1. Since the flow of ALG towards the PEG-rich phases seems to be close to neglectable, the migration of EPL from the PEG phase towards dextran is probably one of the most important factors contributing to the formation of the interface-complexed fibers. This fact may also explain the observed growth of the fibers' walls inwards, which is corroborated by the maintenance of their outer diameter overtime (Figure S5a, Supporting Information), as well as the gradual increase of the thickness of the membrane wall, until full closure of the lumen observed at 60 minutes (Figure S5b, Supporting Information).

The production yield of continuous and non-leaky fibers obtained using 2 and 15 minutes of complexation was assessed. While for non-equilibrated phases, the achievement of high yields of non-leaky fibers depended on the restriction of the complexation time to 2 minutes, the use of equilibrated phases led to a significant improvement of the yield of continuous fibers obtained with 15 minutes complexation (Figure 3d). Moreover, this trend is in agreement with the use of systems closer to the binodal curve (i.e., TL1 and TL2). The thickness of fibers obtained in different TLs was also assessed and compared with samples fabricated in the non-equilibrium system, with different partition coefficients resulting in neglectable changes in the membranes' thickness, both for 2 and 15 minutes complexation (Figure 3e). Overall, the use of equilibrated ATPS improved the production of continuous non-leaky fibers, showcasing thicknesses similar to fibers prepared in non-equilibrated phases, and with increasing production yields for tie lines associated with lower interfacial tensions.

The potential of using the developed tubes as substrates for cell culture was assessed by resuspending mesenchymal stem cells derived from human adipose tissue (hASCs) in phase I (ATPS precursor), and producing the fiber-shaped materials using a syringe-needle manual method under sterile conditions. Mesenchymal stem cells have been considered promising therapeutic cells for the regeneration of damaged tissues. This potential is mainly associated to their differentiation potential into many specific cell types, as well as to paracrine effects characterized by the release of a variety of trophic factors that have been related to their capacity to modulate the immune system, promote cell survival and proliferation, and enhance angiogenesis.[43] Although we previously reported the encapsulation of mesenchymal stem cells derived from the umbilical cord with low cytotoxicity in EPL/alginate spherical millimetric and micrometric capsules[44], we here relied on a higher concentration of the positively charged EPL and continuous ejection forces to prepare membrane-bounded fibers. Despite its positive charge, associated with its antimicrobial potential and often correlated with a cytotoxic potential for several molecules, EPL is considered to have a relatively low toxicity against mammalian cells.[45] A preliminary cytotoxicity assessment for different complexation times showed that times of complexation up to 5 min were compatible with high cell viability (Figure S6, Supporting Information). To potentiate cell adhesion, alginate functionalized with the RGD sequence was used for the assembly of the fibers. This peptide sequence is present in several extracellular matrix proteins, and is responsible for mediating cell adhesion through integrin-binding.[46] The purpose of including alginate-RGD was to further promote cell adhesion throughout the structure at the membrane-level while maintaining the processing requirements for the generation of the material, enabling ALG complexation with EPL molecules. By using

this strategy, we avoided the need for incorporation of external microparticles in the system ‑ a commonly used approach to provide cell anchorage support in cell-laden liquid-core membrane bounded materials ‑, or the formation of multicellular aggregates.[44,47]

The ability of encapsulating adherent cells in the developed biomaterial fibers was assessed using hASCs (**Figure 4**a). The viability of encapsulated cells was monitored by fluorescence microscopy using live/dead staining, and cellular metabolic activity was assessed for 14 days of cell culture (Figure 4b,c). hASCs adhered and showcased a spread morphology in fibers' walls on day 7, and a similar behavior was observed for 14 days of culture, with the formation of an increasing number of interconnected networks with neighboring cells (Figure 4b). Although a statistical decrease in cell metabolic activity was observed after 4 days of culture, cellular activity recovered after 14 days (Figure 3c), indicating the cytocompatibility of the method. The location of cells upon the formation of the coacervate fibers was assessed by imaging techniques. SEM images, as well as optical and fluorescence micrographs, showed that a fraction of cells was incorporated in the polymeric membrane (Figure S7, Supporting Information). In general, cells seemed to be present only in one side of the membrane (the inside part), which did not affect the ability of continuous and stable fibers to be formed. Additionally, the importance of the aqueous separating system as a key element in the formation of intact devices for cell encapsulation procedures was also assessed. While maintaining the same processing conditions, but in the absence of the ATPS precursors, collapsed structures with non-uniform thickness and tendency to undergo localized rupture were obtained. Nonetheless, cell viability was not negatively affected in this setup, although it seems to have driven cell aggregation (Figure S8, Supporting Information). This result reinforces the importance of building structures at the interface of ATPS to achieve high homogeneity and easy of handling.

3. Conclusion

In summary, a straightforward method was established to directly fabricate fiber-shaped materials stable in all-aqueous physiological-relevant conditions, through the interfacial complexation of oppositely charged natural polyelectrolytes. Size-versatile fibers and tubes could be obtained from highly accessible, affordable and off-the-shelf materials, avoiding the use of specifically designed materials.[32,48,49] Our system enables the single-step generation of robust, free- and self-standing flexible materials with arbitrary spatial organization, and features of tubular structures after trimming, enabling the perfusion of liquid fluids. The diameter of the structures could vary from millimeter to micrometer sizes depending on the size of the needle used to extrude the dispersive phase, and mechanical and swelling properties could be easily

tuned by adjusting time of complexation. Optimized polyelectrolyte concentrations, complexation time, pH, and equilibrium status in completely aqueous conditions led to the production of devices with adequate permeability, and with potential to encapsulate delicate cargos and maintain their bioactivity. Mesenchymal stem cells could be easily encapsulated within fiber walls comprising cell adhesive peptide domains, where they adhered and spread for 14 days, indicating that functional features of the developed material can also be controlled.

For the first time, non-spherical materials assembled at the interface of non-equilibrated aqueous phases and ATPS at different equilibrium points are fabricated as self-standing entities, with the ability to be used and handled outside the equilibrated two-phase system. The tube-shape and cytocompatible features of the reported materials enable to foresee potential applications in the biomedical field, enabling its integration into three-dimensional matrices, as well as to be connected to perfusion sources, integrating *in vitro* multichannel fluidics devices.

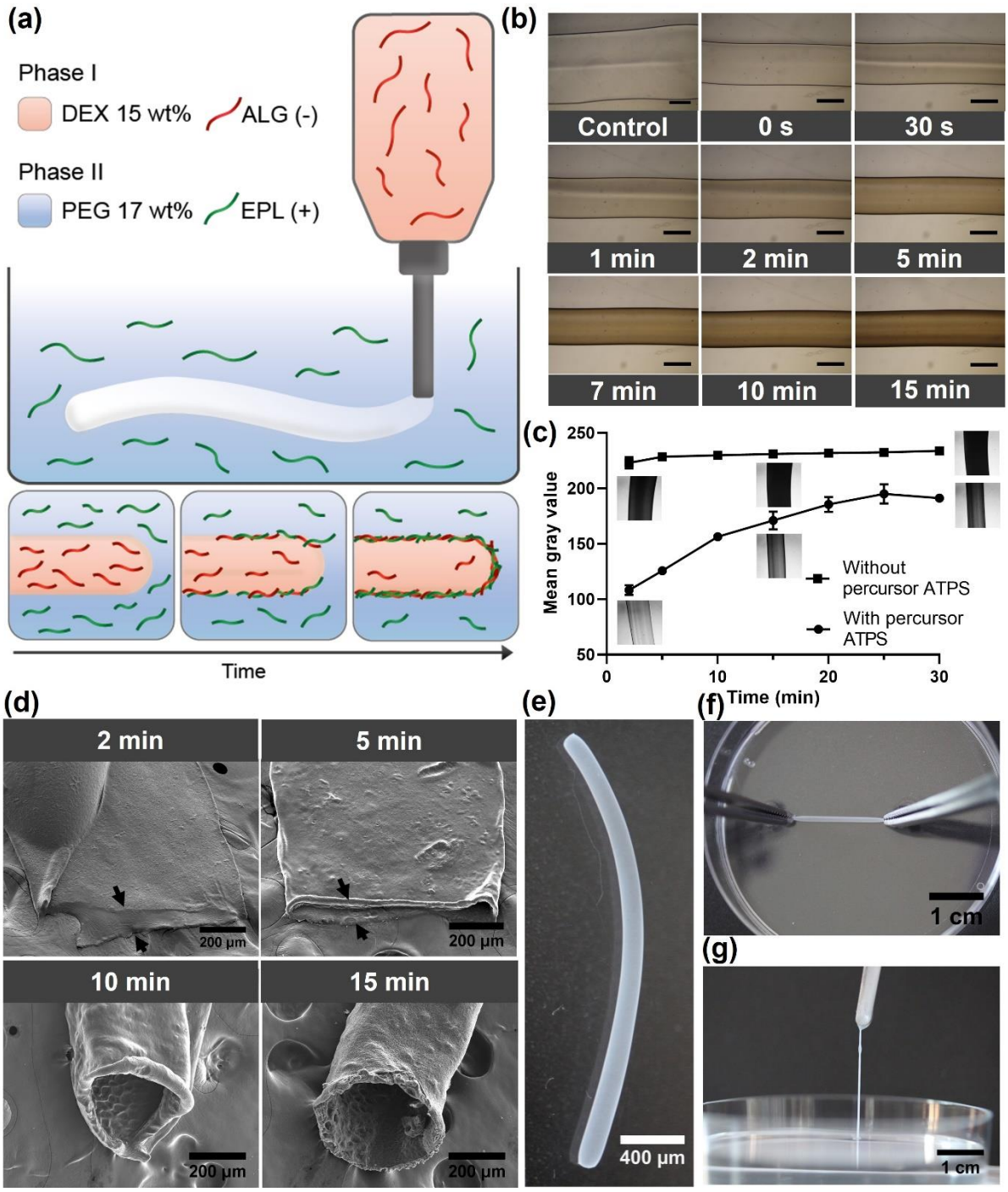

Figure 1. Characteristics of tubule fibers produced in all-aqueous environments. (a) Schematic representation of fiber formation using polyelectrolyte complexation between alginate and ε-poly-L-lysine (EPL) at the interface of an aqueous two-phase system composed of PEG and dextran. (b) Microscopic images showing the darkening of the membrane over time, compared to the control consisting of dextran phase immersed in PEG phase without the polyelectrolytes. Scale bar: 500 µm. (c) Mean gray value over time of fibers produced in the presence and absence of the ATPS precursor (n = 3 replicate fibers). (d) SEM micrographs of cross-sectioned fibers with different complexation times demonstrating hollow features after dehydration. Arrows

indicate upper and lower layers of collapsed structures with 2 and 5 min of complexation. (e) Free-standing fiber material remained intact after 3x washing with PBS. (f,g) The structure was able to be handled with tweezers both in PBS (f) and in air (g).

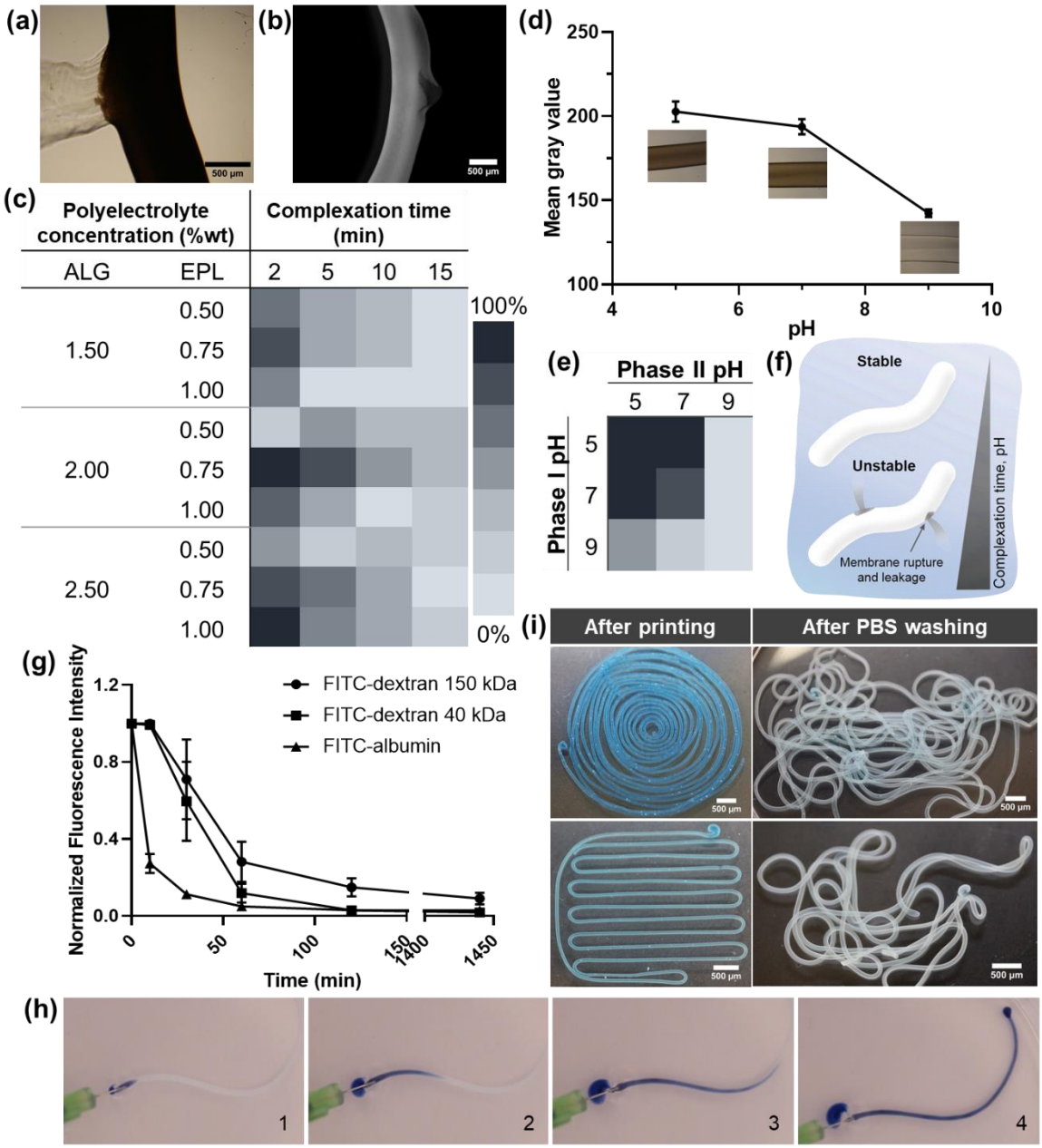

Figure 2. Stability optimization, pH dependency, and system permeability and versatility. Representative images retrieved in a microscope (a) and stereomicroscope (b) of fiber leaking spots after washing steps with PBS. Concentrations of 0.75 wt% and 2 wt% for EPL and ALG, respectively, and 10 min of complexation are shown. (c) Yield calculation of fibers' stability based on their ability to remain intact without leakage after 3x PBS washing, and an overnight incubation period at 37ºC (n = 10 replicate fibers). (d) Mean gray value determined for microscopic images of different fibers produced in a system with a global pH of 5, 7 and 9

(means that both phase I and II were adjusted to the related pH) (n = 5 replicate fibers). (e) Analysis of the yield-related stability and structural integrity of fibers formed in systems with varying phase I and II pH values (n=10 fibers per condition). (f) Graphical scheme representing the increase of complexation time and pH leads to the formation of more unstable fibers related to non-continuities derived from membrane rupture and opening. (g) Normalized fluorescence intensity over time inside the fibers, which were produced in 2 min of complexation and further washed and transferred to a PBS bath solution (n = 20 replicate fibers, excluding leaky fibers). Data indicated as mean ± standard deviation. (h) Time-lapse images from a video, showing the perfusion of a blue dyed liquid solution throughout the structure. (i) Free-form deformability and ability to generate long length fibers with different shapes using an extrusion-based 3D bioprinter. The structures could remain intact after washing with PBS. After printing the fibers are blue due to the addition of a blue dye to visualize the printing procedure.

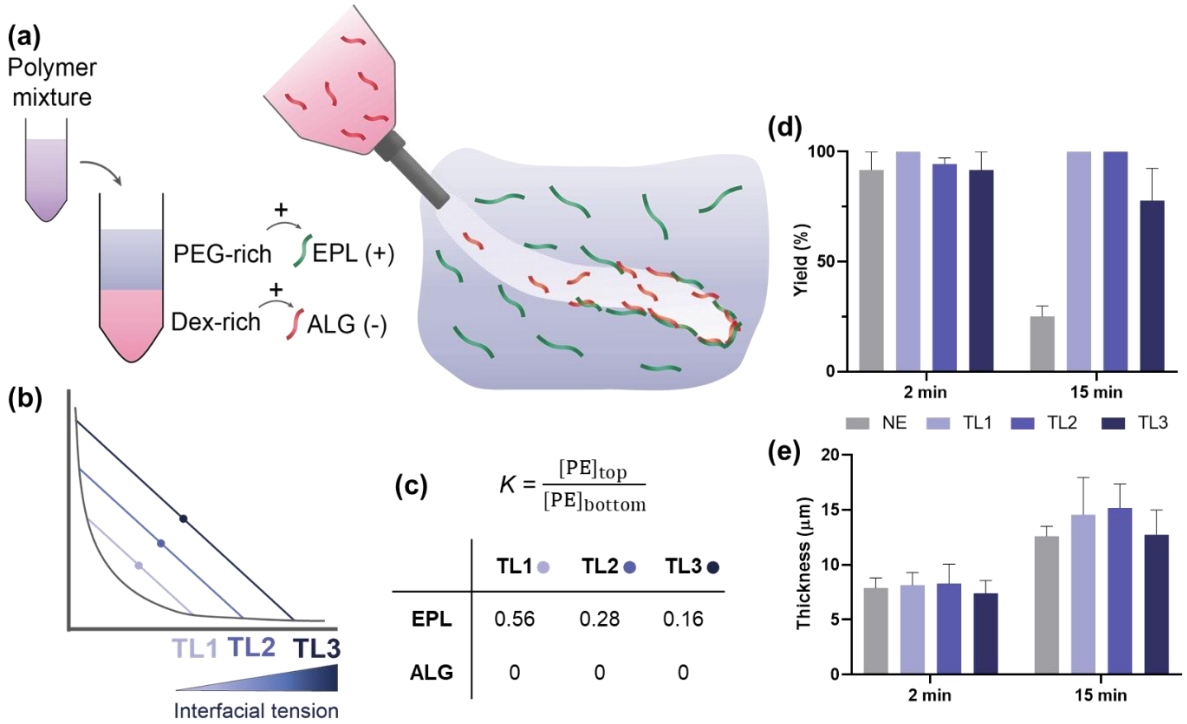

Figure 3. Study of the effect of ATPS equilibrium on the fabrication of coacervate fibers. (a) Schematic representation of the phase separation obtained after mixing PEG and dextran at different mixing points, obtained from (b) tie lines selected from a phase diagram of the ATPS. (c) Partition coefficients calculated for three different tie lines of the system. (d) Yield of fabrication of continuous non-leaky fibers obtained after washing for non-equilibrated precursory ATPS condition (NE), and for the three different equilibrium points (TL1, TL2, and

TL3) (n>24 fibers). (e) Thickness measured for fibers prepared on NE or different ATPS equilibria (n=6).

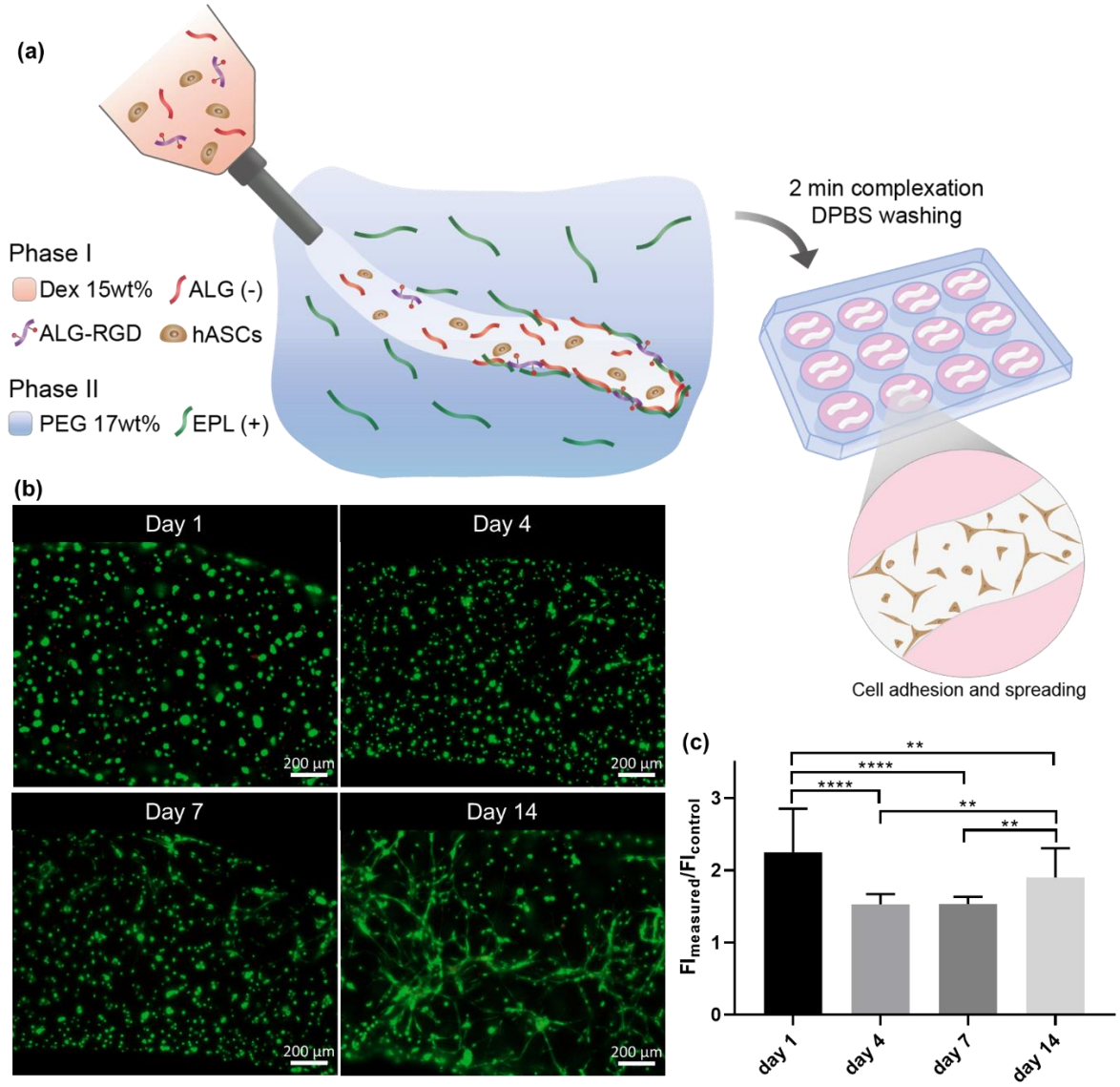

Figure 4. Encapsulation of human adipose-derived stem cells. (a) Schematic representation of the cell encapsulation procedure where hASCs are mixed in phase I also containing alginate functionalized with the RGD domain. Fibers are produced and washed with DPBS after 2 min of complexation, placed on well-plates with appropriate cell culture medium. Cells start to adhere through the fiber material after several days of culture. (b) Live/Dead micrographs of fibers with hASCs after 1, 4, 7 and 14 days of culture. Green: calcein-AM (live), red: PI (dead). (c) Cell metabolic activity measured by the fluorescence intensity using AlamarBlue assay. Samples with size of approximately 0.5 cm long were used (n = 2 independent experiments; 4 replicate fibers/experiment). The values of fluorescence in cell-laden fibers (Fl measured) were

normalized with the fluorescence of non-cell fibers (Fl control). *** and ** indicates statistical significance with $p < 0.0001$ and $p < 0.01$, respectively.

Experimental Section

Materials: Poly(ethylene glycol) (average MW 8000 Da), dextran (from Leuconostoc spp., MW 450,000 – 650,000 Da), sodium alginate from brown algae (MW 120,000-190,000 g moL^{-1}), and phosphate buffered saline (PBS) pellets were purchased from Sigma-Aldrich. ε-Poly-L-lysine (Epolyly®, MW ~ 4700 g mol^{-1}) derived from fermentation of Streptomyces albulus PD-1 was purchased from Handary S.A. (Brussels, Belgium). For cell assays, was used sodium alginate NOVATACHTM MVG GRGDSP (GRGDSP-coupled high MW alginate) which was purchased from NovaMatrix (Sandvika, Norway).

Formation of fibers using ATPS: For experiments using the non-equilibrated ATPS precursor, solutions of 17 wt% poly(ethylene glycol) (PEG) and 15 wt% dextran (DEX) were prepared in PBS.[44] Sodium alginate (ALG) and ε-poly-L-lysine (EPL) were dissolved separately in the DEX 15 wt% and PEG 17 wt% solutions, respectively. In equilibrium conditions, mixtures of dextran and PEG were prepared accordingly to mixture points of the tie lines selected from Liu et al.[42] by dissolving the polymers in PBS. The solutions were left sitting and further centrifugation at 5000 rpm for 15 min to obtain a well separated two-phase system. ALG was dissolved in the DEX-rich inner phase to be extruded, and EPL in the PEG-rich outer/bath phase. Considering that phase volume ratios vary along the same tie line[50], the polymer mixture in each TL was chosen considering the preparation of fibers where a much higher quantity of bath phase (PEG-rich) is needed compared to an extruded filament of inner (DEX-rich) phase. The following initial compositions were used: PEG 7.5 wt% + DEX 3 wt%; PEG 12 wt% + DEX 3 wt%; and PEG 15 wt% + DEX 3 wt% for TL1, TL2 and TL3, respectively.

Fibers could be prepared using a simple manual injection method, where a solution composed of dextran and alginate (phase I) is dispersed through a syringe in a bath solution composed of PEG and EPL (phase II), by moving the syringe in thread-like configurations. To improve the control over the injection flow rate and shape of the structures, a syringe pump (Harvard Apparatus) with assembled syringes with 25 gauge needle was used. A microfluidic fluorinated ethylene-propylene tubing with 0.5 mm of inner diameter (Dolomite) was placed in front of the needles so that the phase was extruded perpendicular to the petri dish containing the bath

solution, using a flow rate of 0.2 mL min^{-1}. The ends of the fibers could be further removed still within the complexation bath by cutting with a spatula, in order to remove irregularities derived from the processing method and produce straight structures with a specific length if required. Since polyelectrolytes were still able to interact inside the complexation bath, the ends spontaneously closed after cutting. After formation, fibers were kept in agitation in an orbital shaker at 30 rpm during a pre-determined complexation time, to prevent the structures from sinking to the bottom of the petri dish due to higher density of phase I compared to the continuous phase II, allowing PE complexation to occur uniformly throughout the entire segment. To test the ability of fibers to be perfused, complexation was interrupted at pre-determined times by removing the bath phase and then washing the fibers with PBS (Sigma-Aldrich). Afterwards, the closed ends were removed using a spatula to leave the fibers with open ends and allow the liquid-core solution to enter/exit. A diluted blue dye solution was injected through one end using a syringe and a small 34 gauge needle.

Scanning electron microscopy: Scanning electron microscopy (SEM) analysis was performed to analyze the morphology and the presence of a hollow lumen in the formed structures. Fibers were produced using the syringe pump method with different complexation times, and were dehydrated with ethanol solutions following a concentration gradient of: 30% (v/v), 50% (v/v), 70% (v/v), 80% (v/v), 90% (v/v), 96% (v/v) and 100% (v/v), by immersing them in these solutions for 15 minutes. To visualize the lumen, transversal cross sections were made using a scalpel blade prior to dehydration. In order to make them conductive, samples underwent gold sputtering for 3 minutes. Samples were then imaged using an Ultra-high Resolution Analytical Scanning Electron Microscope HR-FESEM Hitachi SU-70 (Hitachi, Tokyo, Japan).

Stability optimization: To analyze the stability of the fibers according to the concentration of PE, complexation time and system's pH, the ability of the fibers to resist specific conditions after processing was assessed. Different ALG concentrations (1.5 wt%, 2 wt% and 2.5 wt%) and EPL concentrations (0.5 wt%, 0.75% and 1 wt%) were tested as well as different complexation times, namely 2, 5, 10 or 15 min. The continuous phase was immediately removed after complexation, and PBS was added. This washing step was repeated two additional times until complete removal of the continuous phase. With this procedure, a yield was determined for the fibers that could remain stable without opening or collapsing after the washing steps plus an overnight incubation period at 37°C (Equation 1). Two independent experiments were performed with a total representative number of 10 fibers used for each

condition, using fibers with approximately 1.5 cm long. The formation and structural integrity/stability of the PE fibers were also analyzed for different system pH, namely, 5, 7 and 9, and imagens of the fibers were acquired in a microscope (Primostar, Zeiss), all in the same light conditions. To assess the darkening of the membranes, associated with higher extents of complexation, the mean gray value was determined using ImageJ.

$$Yield\ (\%) = \frac{Number\ of\ stable\ fibers\ after\ 37°C\ overnigth\ incubation}{Total\ of\ produced\ fibers} \times 100 \quad (1)$$

Membrane thickness: Tubular fibers were prepared as described using the syringe pump method and washed after pre-established complexation times. Fiber ends were removed using a spatula. The samples were tilted using tweezers, and observed using optical microscopy (Primostar, Zeiss). Membrane thickness while hydrated was measured using ImageJ.

Permeability characterization: Fluorescein isothiocyanate-dextran (Dextran-FITC, Sigma-Aldrich) with different average molecular weights – 40 and 150 kDa – and albumin-fluorescein isothiocyanate conjugate (albumin-FITC, ~66 kDa), were mixed in phase I (1 mg mL^{-1}). Fibers were prepared using the previously described syringe manual method with 25G needles to mimic the further described cell encapsulation scenario. To determine the release profile of the fluorescently labeled molecules that might diffuse through the fiber membrane, the bath solution was removed after 2 min of complexation, and 10 mL of PBS was added, following PBS washes (30 mL) (x2). 5 fibers with 0.5 cm long were made, in quadruplicates, for each fluorescent molecule. Images were acquired at 0 min (immediately after the first washing step), 10 min, 30 min, 60 min, 120 min and 24 hours in a fluorescence microscope (Axio Imager M2, Carl Zeiss, Germany). Fibers that opened during the process were not considered. The fluorescence intensity was quantified using ImageJ software. For each fiber, the fluorescence intensity was normalized with the fluorescence intensity after the first wash (since it was hypothesized to trigger the higher release of molecules).

Free-form 3D printing: To explore the versatility of the system to produce free-form and long structures, an extrusion 3D bioprinter (Inkredible+, Cellink) was used. A colored food dye was added into aqueous solution of phase I to make the printing procedure visible. The different shapes were fabricated using computer aided design models created in SolidWorks 2020, sliced and converted into a print file using Cellink HeartWare Software which was also used to control the bioprinter. A 22G nozzle was used to extrude the dyed solution under 80 kPa pressure at a

speed of 10-15 mm s^{-1}. The structures were produced after immersing the printing nozzle in a petri dish containing the aqueous solution of PEG and EPL (10 mL).

Determination of the partitioning coefficients of polyelectrolytes. The partitioning coefficient is defined as the ratio between the concentration of a compound in the two immiscible phases at equilibrium.[51,52] Based on previously reported methodologies[28,39], to determine the partition coefficients of ALG and EPL in the different studied ATPS compositions, spectrophotometric methods were used. For EPL, different known concentrations were prepared from a stock solution of EPL 1 wt% in PBS, and the absorbance at 230 nm (where EPL shows a distinctive absorbance signal[53]) was measured using a microplate spectrophotometer to obtain a calibration curve. For the experimental systems, a known concentration of EPL in PBS was added to a mixture of PEG and dextran and, after dissolution of the system, the mixture was left sitting overnight, and then centrifugated at 5000 rpm during 15 min to obtain a fully separated system. A separated system prepared with the same polymer composition without the presence of polyelectrolyte was used as blank for samples. The concentration of EPL in both polymer-rich phases was determined using the previously obtained calibration curve, and the partitioning coefficient was calculated as follows (Equation 2):

$$K = \frac{[PE]_{top}}{[PE]_{bottom}} \quad (2)$$

Where $[PE]_{top}$ and $[PE]_{bottom}$ is the concentration of the polyelectrolyte in the top and bottom phase, respectively.

A similar procedure was applied to determine the partitioning coefficient of ALG. A method based on the complexation of ALG with a cationic blue dye (1,9-dimethyl methylene blue (DMMB, Sigma-Aldrich) (adapted from[54,55]) was applied. Briefly, solutions for the calibration curve and experimental phase-separated systems (samples and blank) were incubated with a 1 mM DMMB solution (in water) (1:25) for 45 min. The absorbance was measured at 520 and 650 nm to determine the 520/650 nm absorbance ratio. ALG concentrations were determined, and the partition coefficient calculated using equation 2. The initial compositions of PEG and dextran for the separation in PEG-rich and dextran-rich phases in conditions TL1, TL2 and TL3 were chosen from the phase diagram previously reported by Liu et al.[42], considering an equal phase volume ratio (at the center of the TL). The following compositions were used: PEG 5.1 wt% + DEX 8 wt%: PEG 7 wt% + DEX 12 wt%; and PEG 8.6 wt% + DEX 15 wt% for the samples TL1, TL2 and TL3, respectively.

Cell culture and encapsulation: The cytocompatibility of PE fibers was evaluated using human adipose-derived mesenchymal stem cells (hASCs) (purchased from LGC Standards, ATCC) and were cultured in α-MEM, supplemented with 10% (v/v) fetal bovine serum (FBS, ThermoScientific) and 1% antibiotic/antimycotic (ThermoScientific). Cells were used in passages between 6 to 8. Cell suspensions were prepared after trypsinization and were encapsulated in the phase to be dispersed containing the ALG 2 wt%. To promote cell adhesion, alginate functionalized with the cell adhesion peptide arginine-glycine-aspartate (ALG-RGD) was used at a concentration of 0.5 wt%. Both solutions containing the phase-forming polymers and PEs were sterilized. For that, ATPS phases containing the dissolved polymers were filtered using sterile 0.2 μm pore-sized filters, alginate and EPL reagents were exposed to UV light during 40 min and ALG-RGD during 20 min. The sterile polyelectrolytes were added to the filtered solutions to dissolution using autoclaved stirring magnets. A syringe containing the phase with cells ($10 \times 10^6\ cells/mL$) was manually injected in the phase containing PEG and EPL to facilitate the processing method. After 2 min of complexation, DPBS was added (x3), and fibers were transferred to a DPBS solution (30 mL) and then to the appropriate cell culture medium. Cell encapsulated fibers were maintained in incubators with controlled temperature (37ºC) and 5% CO2. For the comparison of structures being formed with and without the presence of the ATPS, the fibers were produced as previously described in sterile conditions, and the same cell density of $10 \times 10^6\ cells/mL$ was used in both conditions, but in this case, MC3T3 cell lineage cultured also in α-MEM medium with the appropriate supplementation, was used.

Cell viability assays: The cell viability of cell-laden fibers was analyzed by live/dead assay (Invitrogen, USA) and Alamar Blue® Cell Viability assay at different time points. Both assays were performed in accordance with manufacturer instructions. To analyze live and dead cells at pre-determined timepoints, fibers were incubated in cell culture medium with propidium iodide (PI) (Thermo Fisher Scientific) and Calcein-AM solution (Thermo Fisher Scientific) at concentration of 1 μL mL^{-1} and 2 μL mL^{-1}, respectively, during 10 min at 37°C. Fibers were washed with culture medium and examined in an upright widefield fluorescence microscope (Axio Imager M2, Carl Zeiss, Germany). The AlamarBlue® assay (Thermo Fisher Scientific) was used to access metabolic activity of encapsulated cells. Cell encapsulated fibers with approximately 0.5 cm long were placed in a 48 well-plate with 1.2 cm of diameter per well. AlamarBlue™ reagent was added to the cell culture medium (1:10), with an incubation period

of 8.5 hours. Fluorescent measurements (λexcitation: 540 nm, λemission: 600 nm) were performed in a Synergy HTX microplate reader using a 96-well black-clear bottom plate. A representative number of four fibers per independent experience were used for each assay at the different timepoints.

For cell nuclei identification in the membranes, cell-laden fibers were fixed with cold methanol for 10 min at -20ºC. Afterwards, the structures were washed with PBS and ruptured with up and down movements using a micropipette. Fiber fragments were incubated with 4',6-Diamidine-2'-phenylindole dihydrochloride (DAPI, ThermoScientific, 1 µg/mL) at room temperature, and cell nuclei visualized in a fluorescence microscope.

Statistical analysis: GraphPad Prism 8 was applied for data statistical analysis, and results are presented as mean ± standard deviation. Statistical significance between the groups was determined by multiple t tests using one-way and two-way analysis of variance (ANOVA), considering a statistically significant difference if $p < 0.05$.

Supporting Information

Supporting Information is available from the Wiley Online Library or from the author.

Acknowledgements

This work was financially supported by the European Research Council grant agreement ERC-2014-ADG-669858 (project ATLAS), by the Programa Operacional Competitividade e Internacionalizaçao, in the component FEDER, and by national funds (OE) through FCT/MCTES, in the scope of the projects 'TranSphera' (PTDC/BTM-ORG/30770/2017) and "CellFi" (PTDC/BTM-ORG/3215/2020). This work was developed within the scope of the project CICECO-Aveiro Institute of Materials, UIDB/50011/2020, UIDP/50011/2020 & LA/P/0006/2020, financed by national funds through the FCT/MEC (PIDDAC). M. B. Oliveira acknowledges the individual contract CEECIND/03605/2017. FCT also financially supported this work through individual doctoral grant 2021.07435.BD of Raquel C. Gonçalves.

Conflict of interest

The authors declare no conflict of interest.

Data Availability Statement

The raw data required to reproduce these findings are available from the authors upon request.

Received: ((will be filled in by the editorial staff))
Revised: ((will be filled in by the editorial staff))
Published online: ((will be filled in by the editorial staff))

References

[1] Z. J. Meng, W. Wang, R. Xie, X. J. Ju, Z. Liu, L. Y. Chu, *Lab on a Chip* **2016**, *16*, 2673.
[2] C. R. Correia, R. L. Reis, J. F. Mano, *Advanced Healthcare Materials* **2018**, *7*, 1701444.
[3] C. R. Correia, S. Nadine, J. F. Mano, *Advanced Functional Materials* **2020**, *30*, 1908061.
[4] G. Luo, Y. Yu, Y. Yuan, X. Chen, Z. Liu, T. Kong, *Advanced Materials* **2019**, *31*, 1904631.
[5] A. R. Sousa, C. Martins-Cruz, M. B. Oliveira, J. F. Mano, *Advanced Materials* **2020**, *32*, DOI 10.1002/adma.201906305.
[6] K. A. DiVito, M. A. Daniele, S. A. Roberts, F. S. Ligler, A. A. Adams, *Biomaterials* **2017**, *138*, 142.
[7] H. Wang, H. Liu, X. Zhang, Y. Wang, M. Zhao, W. Chen, J. Qin, *ACS Applied Materials and Interfaces* **2021**, *13*, 3199.
[8] Y. Zhu, L. Wang, F. Yin, Y. Yu, Y. Wang, H. Liu, H. Wang, N. Sun, H. Liu, J. Qin, *Integrative Biology* **2017**, *9*, 774.
[9] H. Savoji, L. Davenport Huyer, M. H. Mohammadi, B. F. Lun Lai, N. Rafatian, D. Bannerman, M. Shoaib, E. R. Bobicki, A. Ramachandran, M. Radisic, *ACS Biomaterials Science & Engineering* **2020**, *6*, 1333.
[10] Q. Gao, Y. He, J. zhong Fu, A. Liu, L. Ma, *Biomaterials* **2015**, *61*, 203.
[11] W. Jia, P. S. Gungor-Ozkerim, Y. S. Zhang, K. Yue, K. Zhu, W. Liu, Q. Pi, B. Byambaa, M. R. Dokmeci, S. R. Shin, A. Khademhosseini, *Biomaterials* **2016**, *106*, 58.
[12] Q. Pi, S. Maharjan, X. Yan, X. Liu, B. Singh, A. M. van Genderen, F. Robledo-Padilla, R. Parra-Saldivar, N. Hu, W. Jia, C. Xu, J. Kang, S. Hassan, H. Cheng, X. Hou, A. Khademhosseini, Y. S. Zhang, *Advanced Materials* **2018**, *30*, 1706913.
[13] C. Li, X. Han, Z. Ma, T. Jie, J. Wang, L. Deng, W. Cui, *Advanced Healthcare Materials* **2021**, 2101836.
[14] W. Feng, Y. Chai, J. Forth, P. D. Ashby, T. P. Russell, B. A. Helms, *Nature Communications* **2019**, *10*, 1095.
[15] S. Shi, T. P. Russell, *Advanced Materials* **2018**, *30*, 1800714.

675 [16] J. Forth, P. Y. Kim, G. Xie, X. Liu, B. A. Helms, T. P. Russell, *Advanced Materials* **2019**, *31*, 1806370.
677 [17] Y. Chao, H. C. Shum, *Chemical Society Reviews* **2020**, *49*, 114.
678 [18] A. G. Teixeira, R. Agarwal, K. R. Ko, J. Grant-Burt, B. M. Leung, J. P. Frampton, *Advanced Healthcare Materials* **2018**, *7*, 1701036.
680 [19] L. Zhang, L. H. Cai, P. S. Lienemann, T. Rossow, I. Polenz, Q. Vallmajo-Martin, M. Ehrbar, H. Na, D. J. Mooney, D. A. Weitz, *Angewandte Chemie - International Edition* **2016**, *55*, 13470.
683 [20] M. Kim, S. J. Yeo, C. B. Highley, J. A. Burdick, P. J. Yoo, J. Doh, D. Lee, *ACS Nano* **2015**, *9*, 8269.
685 [21] S. D. Hann, T. H. R. Niepa, K. J. Stebe, D. Lee, *ACS Applied Materials and Interfaces* **2016**, *8*, 25603.
687 [22] S. D. Hann, D. Lee, K. J. Stebe, *Physical Chemistry Chemical Physics* **2017**, *19*, 23825.
688 [23] Y. Zou, J. Song, X. You, J. Yao, S. Xie, M. Jin, X. Wang, Z. Yan, G. Zhou, L. Shui, *ACS Applied Materials and Interfaces* **2019**, *11*, 21227.
690 [24] H. Liu, Y. Wang, H. Wang, M. Zhao, T. Tao, X. Zhang, J. Qin, *Advanced Science* **2020**, *7*, 1903739.
692 [25] G. Xie, J. Forth, Y. Chai, P. D. Ashby, B. A. Helms, T. P. Russell, *Chem* **2019**, *5*, 2678.
693 [26] J. Fu, J. B. Schlenoff, *J Am Chem Soc* **2016**, *138*, 980.
694 [27] R. H. Tromp, R. Tuinier, M. Vis, *Physical Chemistry Chemical Physics* **2016**, *18*, 30931.
695 [28] Q. Ma, Y. Song, J. W. Kim, H. S. Choi, H. C. Shum, *ACS Macro Letters* **2016**, *5*, 666.
696 [29] A. B. Kayitmazer, *Advances in Colloid and Interface Science* **2017**, *239*, 169.
697 [30] T. R. Cox, J. T. Erler, *Disease Models and Mechanisms* **2011**, *4*, 165.
698 [31] S. Park, R. Barnes, Y. Lin, B. jin Jeon, S. Najafi, K. T. Delaney, G. H. Fredrickson, J. E. Shea, D. S. Hwang, S. Han, *Communications Chemistry* **2020**, *3*, 83.
700 [32] K. E. Inostroza-Brito, E. Collin, O. Siton-Mendelson, K. H. Smith, A. Monge-Marcet, D. S. Ferreira, R. P. Rodríguez, M. Alonso, J. C. Rodríguez-Cabello, R. L. Reis, F. Sagués, L. Botto, R. Bitton, H. S. Azevedo, A. Mata, *Nature Chemistry* **2015**, *7*, 897.
703 [33] A. M. Díez-Pascual, P. S. Shuttleworth, *Materials* **2014**, *7*, 7472.
704 [34] A. M. Díez-Pascual, P. S. Shuttleworth, *Materials* **2014**, *7*, 7472.
705 [35] F. Loosli, L. Vitorazi, J. F. Berret, S. Stoll, *Water Research* **2015**, *80*, 139.
706 [36] M. G. Carneiro-Da-Cunha, M. A. Cerqueira, B. W. S. Souza, J. A. Teixeira, A. A. Vicente, *Carbohydrate Polymers* **2011**, *85*, 522.

[37] S. C. Shukla, A. Singh, A. K. Pandey, A. Mishra, *Biochemical Engineering Journal* **2012**, *65*, 70.

[38] T. Yoshida, T. Nagasawa, *Applied Microbiology and Biotechnology* **2003**, *62*, 21.

[39] Q. Ma, H. Yuan, Y. Song, Y. Chao, S. Y. Mak, H. C. Shum, *Soft Matter* **2018**, *14*, 1552.

[40] K. Raj M, S. Chakraborty, *Journal of Applied Polymer Science* **2020**, *137*, 48958.

[41] C. L. Thompson, S. Fu, M. M. Knight, S. D. Thorpe, *Frontiers in Bioengineering and Biotechnology* **2020**, *8*, 602646.

[42] Y. Liu, R. Lipowsky, R. Dimova, *Langmuir* **2012**, *28*, 3831.

[43] Y. Fu, L. Karbaat, L. Wu, J. Leijten, S. K. Both, M. Karperien, *Tissue Engineering - Part B: Reviews* **2017**, *23*, 515.

[44] S. Vilabril, S. Nadine, C. M. S. S. Neves, C. R. Correia, M. G. Freire, J. A. P. Coutinho, M. B. Oliveira, J. F. Mano, *Advanced Healthcare Materials* **2021**, 2100266.

[45] M. Hyldgaard, T. Mygind, B. S. Vad, M. Stenvang, D. E. Otzen, R. L. Meyer, *Applied and Environmental Microbiology* **2014**, *80*, 7758.

[46] S. L. Bellis, *Biomaterials* **2011**, *32*, 4205.

[47] C. R. Correia, R. P. Pirraco, M. T. Cerqueira, A. P. Marques, R. L. Reis, J. F. Mano, *Scientific Reports* **2016**, *6*, 21883.

[48] Y. Wu, B. O. Okesola, J. Xu, I. Korotkin, A. Berardo, I. Corridori, F. L. P. di Brocchetti, J. Kanczler, J. Feng, W. Li, Y. Shi, V. Farafonov, Y. Wang, R. F. Thompson, M. M. Titirici, D. Nerukh, S. Karabasov, R. O. C. Oreffo, J. Carlos Rodriguez-Cabello, G. Vozzi, H. S. Azevedo, N. M. Pugno, W. Wang, A. Mata, *Nature Communications* **2020**, *11*, 1182.

[49] Y. Wu, G. M. Fortunato, B. O. Okesola, F. L. P. Di Brocchetti, R. Suntornnond, J. Connelly, C. De Maria, J. C. Rodriguez-Cabello, G. Vozzi, W. Wang, A. Mata, *Biofabrication* **2021**, *13*, 035027.

[50] J. F. B. Pereira, J. A. P. Coutinho, *Liquid-Phase Extraction* **2020**, 157.

[51] A. L. Grilo, M. R. Aires-Barros, A. M. Azevedo, *Separation and Purification Reviews* **2016**, *45*, 68.

[52] M. Iqbal, Y. Tao, S. Xie, Y. Zhu, D. Chen, X. Wang, L. Huang, D. Peng, A. Sattar, M. A. B. Shabbir, H. I. Hussain, S. Ahmed, Z. Yuan, *Biological Procedures Online* **2016**, *18*, 18.

[53] Y. Meng, Q. Xue, J. Chen, Y. Li, Z. Shao, *Journal of Dairy Science* **2022**, *105*, 3746.

[54] J. P. Halle, D. Landry, A. Fournier, M. Beaudry, F. A. Leblond, *Cell Transplantation* **1993**, *2*, 429.

[55] J. C. Richardson, P. W. Dettmar, F. C. Hampson, C. D. Melia, *European Journal of Pharmaceutics and Biopharmaceutics* **2004**, *57*, 299.